

# More on the rainbow chain: entanglement, space-time geometry and thermal states

Javier Rodríguez-Laguna<sup>1</sup>, Jérôme Dubail<sup>2</sup>, Giovanni Ramírez<sup>3</sup>, Pasquale Calabrese<sup>4</sup>, Germán Sierra<sup>5</sup>

<sup>1</sup> Dto. Física Fundamental, Universidad Nacional de Educación a Distancia (UNED), Madrid, Spain.

<sup>2</sup> CNRS & IJL-UMR, Université de Lorraine, F-54506 Vandoeuvre-les-Nancy, France.

<sup>3</sup> Instituto de Investigación, Escuela de Ciencias Físicas y Matemáticas, Universidad de San Carlos de Guatemala, Guatemala

<sup>4</sup> SISSA and INFN, Via Bonomea 265, 34136 Trieste, Italy

<sup>5</sup> Instituto de Física Teórica (IFT), UAM-CSIC, Madrid, Spain

**Abstract.** The rainbow chain is an inhomogenous exactly solvable local spin model that, in its ground state, displays a half-chain entanglement entropy growing linearly with the system size. Although many exact results about the rainbow chain are known, the structure of the underlying quantum field theory has not yet been unraveled. Here we show that the universal scaling features of this model are captured by a massless Dirac fermion in a curved space-time with constant negative curvature  $R = -h^2$  ( $h$  is the amplitude of the inhomogeneity). This identification allows us to use recently developed techniques to study inhomogeneous conformal systems and to analytically characterise the entanglement entropies of more general bipartitions. These results are carefully tested against exact numerical calculations. Finally, we study the entanglement entropies of the rainbow chain in thermal states, and find that there is a non-trivial interplay between the rainbow effective temperature  $T_R$  and the physical temperature  $T$ .

## 1. Introduction

In recent years there has been an intense activity to study extended quantum systems from the perspective of entanglement [1, 2, 3, 4]. This concept is certainly not new but it is moving to central stage in several areas of physics such as condensed matter physics, quantum optics, quantum field theory and quantum gravity. Furthermore the entanglement entropies recently became accessible to cold atomic experiments [5, 6] and there are a number of theoretical proposals to access many other universal features of entanglement [7, 8, 9, 10, 11, 12]. Consequently, it is of fundamental importance to characterise the entanglement properties of many-body systems, especially in those situations that can be realised experimentally. More and more attention has been recently drawn to inhomogeneous many-body systems in one spatial dimension for a twofold reason: on the one hand, in nature inhomogeneities are more the rule rather than the exception, on the other hand, in some of these models the entanglement properties exhibit interesting departures from the laws satisfied by uniform models. For example, spin chains with quenched disorder in the couplings are not conformal invariant but show, in average, logarithmic entanglement entropies [13, 14, 15, 16, 17, 18], similarly to the uniform conformal case [19, 20, 21, 22] but with a different prefactor. Lattice models with couplings that increase exponentially with the position show analogies with Wilson’s RG approach to the Kondo problem [23]. Hyperbolic couplings have been introduced to reduce the effect of the boundary in estimating the energy of the excited states that become weakly bounded around the centre of the system [24, 25]. Finally, and more importantly for this manuscript, spin chains with couplings that decrease exponentially moving away from the centre of the system give rise to an entanglement scaling with volume of the subsystem even in the ground state [26, 27, 28], resulting in a very anomalous behaviour compared to uniform models.

The similarity between models with smoothly varying couplings and quantum field theories in curved space-times has been put forward in Refs. [29, 30], with potential cold atom realisations in sight. In addition to those proposals for tabletop experiments that mimic effects from high-energy physics, there is another good reason for exploring the relevance of quantum field theory in curved space for the physics of ultracold quantum gases. Most experimental setups involve trapping potentials, often harmonic ones, that result in inhomogeneous density profiles in the models one wants to simulate; in fact, the presence of non-uniform potential wells, or background electromagnetic fields, is the rule rather than the exception. It was pointed out very recently [31], in the study of non-interacting fermion gases in 1+1 dimensions, that the inhomogeneity generated by the trapping potential are captured by quantum field theory in curved space-time.

It is thus of great interest to find a general framework where we can study the entanglement properties of those inhomogeneous systems. The goal of this paper is to apply the techniques of Ref. [31] to the *rainbow* model [26, 27, 28]. In this way, we will understand its entanglement properties and its geometrical significance. The paper is organised as follows. In section 2 we review the main properties of the rainbow chain. In section 3 we carry out the continuum limit of the rainbow model in its Lagrangian formulation, studying in full details the resulting space-time geometry. In section 4 we provide the general CFT expressions of the Rényi entanglement entropies for an arbitrary block of spins, both in the case of a block starting from one end of the chain and of a block with endpoints in the bulk of the system. The corresponding

analytical expressions are carefully verified numerically for several system sizes and inhomogeneity amplitudes, providing in some cases also conjectures for the leading correction to scaling. In section 5 we numerically study the entanglement entropy at non-zero temperature finding an interesting interplay with the effective rainbow temperature. Finally, in section 6 we present our conclusions and some possible prospects.

## 2. Review of the rainbow chain

To define the rainbow model, we consider a chain with  $2L$  sites labelled by the half-odd integers,  $m = \pm\frac{1}{2}, \pm\frac{3}{2}, \dots, \pm(L - \frac{1}{2})$ . Let  $c_m$  and  $c_m^\dagger$  denote the annihilation and creation operators of a spinless fermion at the site  $m$ . The Hamiltonian is [26, 27, 28]

$$H = -\frac{J}{2}c_{\frac{1}{2}}^\dagger c_{-\frac{1}{2}} - \frac{J}{2} \sum_{m=\frac{1}{2}}^{L-\frac{3}{2}} e^{-hm} \left[ c_m^\dagger c_{m+1} + c_{-m}^\dagger c_{-(m+1)} \right] + \text{h.c.}, \quad (1)$$

where  $J > 0$  sets the scale of the hopping parameters, and  $h \geq 0$  characterises the inhomogeneity of the hopping amplitudes. After a Jordan-Wigner transformation Eq. (1) becomes the Hamiltonian of an inhomogeneous spin-1/2  $XX$  chain [26]. The case  $h = 0$  corresponds to the standard uniform Hamiltonian of a spinless free fermion (tight binding model) with open boundary conditions. Its low energy properties are captured by a CFT with central charge  $c = 1$ : the massless Dirac fermion theory, or equivalently (upon bosonization) a Luttinger liquid with Luttinger parameter  $K = 1$ . The ground state of the Hamiltonian (1) has been studied in the strong and in the weak inhomogeneity limits [26, 27, 28]. In the former case, i.e.  $h \gg 1$ , the application of the Dasgupta-Ma real space renormalisation group [33] yields a ground state formed by spin singlets between the sites  $k$  and  $-k$ , for  $k = \frac{1}{2}, \dots, L - \frac{1}{2}$  (in the  $XX$  version of the Hamiltonian). Fig. 1 shows a picture of the ground state that resembles a rainbow (the colours are associated to the energies required to break the bonds, which are proportional to  $e^{-2mh}$ , and so red shifting with  $|m|$ ).

In this paper we will be mainly interested in the characterisation of the block entanglement entropies in the ground state of the rainbow chain (1). Given a block  $A$  formed by  $\ell$  contiguous spins, the Rényi entanglement entropies are defined as

$$S_n = \frac{1}{1-n} \ln \text{Tr}(\rho_A^n), \quad (2)$$

where  $\rho_A \equiv \text{Tr}_{\bar{A}} \rho$  is the reduced density matrix of  $A$  and  $n$  is the order of the Rényi entropy which can be an arbitrary real number. For  $n \rightarrow 1$ ,  $S_n$  reduces to the von Neumann entropy of the subsystem, which is usually referred to as entanglement entropy, and that will be the main quantity of interest also for us. In the following we will simply refer to  $S_1$  as  $S$ , i.e. every time that the Rényi index is missing, we implicitly assume to consider the von Neumann entropy. It is however important to characterise the Rényi entropies for general  $n$ , indeed their knowledge for arbitrary  $n$  gives access to the full spectrum of the reduced density matrix [32]. Given that the rainbow chain is a free fermionic model, one can use standard techniques [34] to evaluate the entanglement entropies for finite (but also very large)  $L$ , as already done in [26, 27, 28].

A fundamental property of the entanglement entropy is that, in the ground state of gapped models, it satisfies the so-called area law [2, 35, 36], i.e. when increasing the subsystem size it scales like the area of  $A$ , in contrast with the volume law of standard

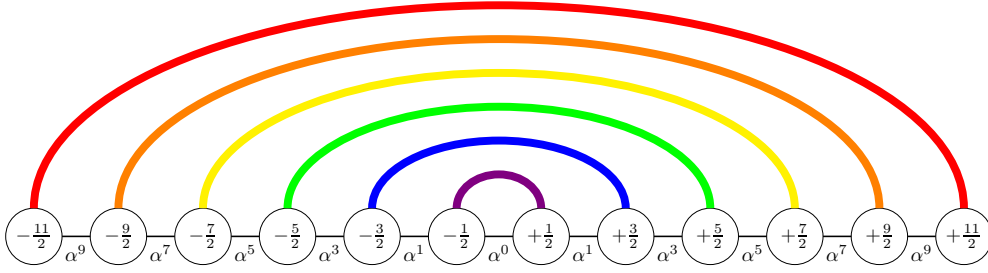


**Figure 1.** Rainbow state showing the  $(-k, +k)$  bonds above the central link. Given that each bond contributes as  $\ln 2$  to the entanglement entropy, the one between the left and the right halves of the chain is  $L \ln 2$ .

thermodynamic entropy at finite temperature. In one spatial dimension, the area law means that the entanglement entropies saturate when increasing the block size; this was proven rigorously by Hastings [37].

For gapless systems, there are many known fundamental examples where the area law breaks down, including logarithmic violations in conformal field theories [19, 20, 21, 22], systems with quenched disorder [13, 14, 15, 16, 17, 18], Fermi gases in arbitrary dimension [38, 39, 40] and many more. Conversely, an unexpected result was the one by Vitigliano *et al.* [26] showing that the rainbow state (i.e. the ground state of the rainbow model) breaks maximally the area law in the limit  $h \gg 1$ . Indeed, since any singlet shared between one block and its complement contribute to the entanglement entropy as  $\ln 2$ , it is clear from Fig. 1 that the half-chain entanglement entropy (i.e. between the left and right blocks) of this state is  $S = L \ln 2$ , which is the highest value it can take for a subsystem containing  $L$  qubits. This valence bond state becomes the exact ground state of the Hamiltonian (1) in the limit  $h \rightarrow \infty$ , but several of its properties persist for all values of  $h$ , in particular the linear dependence on  $L$  of the half-block entropy with a coefficient that depends on  $h$  and it is always smaller than  $\ln 2$ .

In the weak inhomogeneity limit  $h \ll 1$ , it has been shown that the low energy physics of (1) is described by the Hamiltonian of two chiral fermions  $\psi_L$  and  $\psi_R$  of the form [28]

$$H \simeq iJa \int_{-aL}^{aL} dx e^{-\frac{h|x|}{a}} \left[ \psi_R^\dagger \partial_x \psi_R - \psi_L^\dagger \partial_x \psi_L - \frac{h}{2a} \text{sign}(x) (\psi_R^\dagger \psi_R - \psi_L^\dagger \psi_L) \right], \quad (3)$$

where  $a$  is the lattice spacing and  $x = ma$  is the position. The fields  $\psi_{L,R}(x)$  are the slow varying modes of the fermion operator  $c_m$  expanded around the Fermi momenta  $\pm k_F$  (at half filling  $k_F = \pi/(2a)$ )

$$\frac{c_m}{\sqrt{a}} \simeq e^{ik_F x} \psi_L(x) + e^{-ik_F x} \psi_R(x). \quad (4)$$

The continuum limit is defined by the equations  $a \rightarrow 0$ ,  $h \rightarrow 0$  and  $L \rightarrow \infty$ , with  $h/a$  and  $aL$  kept constant. In the rest of the paper, we rename  $h/a \rightarrow h$  and  $aL \rightarrow L$  such that  $h$  and  $L$  acquire the dimensions of  $\text{length}^{-1}$  and  $\text{length}$  respectively. In Eq. (3), the fields  $\psi_{L,R}$  are decoupled in the bulk, however they are coupled by the boundary conditions [28]

$$\psi_R(\pm L) = \mp i \psi_L(\pm L). \quad (5)$$

In reference [28] it was noticed that Eq. (3) can be transformed into the Hamiltonian of a uniform model by the change of variable

$$\tilde{x} = \text{sign}(x) \frac{e^{h|x|} - 1}{h}, \quad (6)$$

that maps the interval  $x \in [-L, L]$  into the interval  $\tilde{x} \in [-\tilde{L}, \tilde{L}]$  where

$$\tilde{L} = \frac{e^{hL} - 1}{h}, \quad (7)$$

plays the role of an effective half-length. The fermion fields in the variable  $\tilde{x}$  transform as

$$\tilde{\psi}_{R,L}(\tilde{x}) = \left( \frac{d\tilde{x}}{dx} \right)^{-1/2} \psi_{R,L}(x) = e^{-h|x|/2} \psi_{R,L}(x), \quad (8)$$

that plugged into Eq. (3) gives

$$H \simeq iJ \int_{-\tilde{L}}^{\tilde{L}} d\tilde{x} \left[ \tilde{\psi}_R^\dagger \partial_{\tilde{x}} \tilde{\psi}_R - \tilde{\psi}_L^\dagger \partial_{\tilde{x}} \tilde{\psi}_L \right]. \quad (9)$$

The change of variables (8) also changes the integration measure of the path integral, so that the transformed fermion is not living anymore in flat space-time, unlike Eq. (9) could erroneously suggest. Nevertheless, this equation was used heuristically in [28] to propose an expression for the half-chain entanglement of the rainbow chain. The trick was to take the entanglement entropy of a homogeneous open chain in CFT [21]

$$S_{\text{CFT}}(L) = \frac{c}{6} \ln(L) + c', \quad (10)$$

with  $c = 1$ , and replace  $L$  by  $\tilde{L}$ , to obtain

$$S(L) = \frac{c}{6} \ln \left( \frac{e^{hL} - 1}{h} \right) + c'. \quad (11)$$

A comparison of this prediction with numerical data is displayed in Fig. 2, for small values of  $h$ , and the agreement is perfect.

In the limit  $hL \ll 1$ , Eq. (11), reproduces the usual CFT behaviour (10), but for  $hL \gg 1$  the entropy behaves extensively

$$S(L) \approx \frac{c}{6} hL, \quad (12)$$

in close analogy with the thermal behaviour of the entanglement entropy of an open system in CFT [21]

$$S_{\text{CFT}}(L, T) \approx \frac{c}{6} \ln \left( \frac{\sinh(2\pi LT)}{\pi T} \right) \rightarrow \frac{c}{3} \pi T L, \quad (13)$$

in the limit where  $TL \gg 1$ . The comparison between Eqs. (12) and (13) suggests (in the limit  $hL \gg 1$ ) a thermal interpretation of the rainbow state with an effective temperature proportional to  $h$

$$T_R = \frac{h}{2\pi} \quad (14)$$

for  $T_R L \gg 1$ .

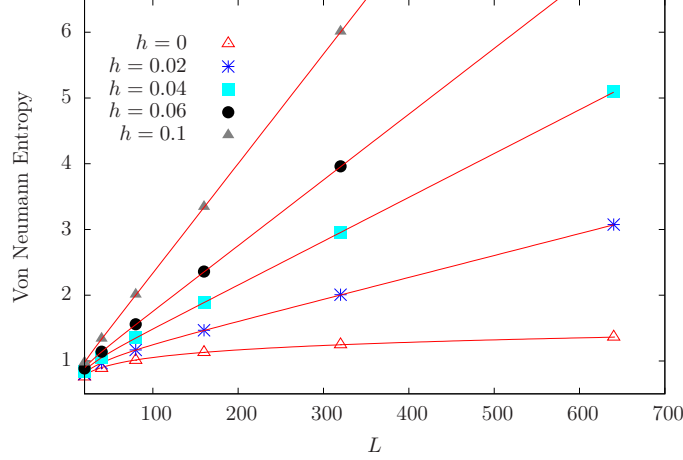


**Figure 2.** Half-chain entanglement entropy for the rainbow model. The figure reports the comparison between exact numerical data (symbols) and the theoretical prediction (11) (lines) for different values of  $L$  and  $h$ . The agreement is perfect in the considered regime of small  $h$ .

### 3. The Rainbow model as a Dirac fermion in curved space-time

In this section we show that the rainbow Hamiltonian can be obtained from the action of a massless Dirac fermion in a curved space-time. We provide a derivation of this result using the covariant formalism of relativistic field theory with Minkowski signature. The Lagrangian associated to the Hamiltonian (3) is

$$\begin{aligned} \mathcal{L} = & \psi_-^\dagger \partial_0 \psi_- + \psi_+^\dagger \partial_0 \psi_+ + e^{-h|x^1|} \left( \psi_-^\dagger \partial_1 \psi_- - \psi_+^\dagger \partial_1 \psi_+ \right) \\ & + \frac{h}{2} \text{sign}(x^1) e^{-h|x^1|} (\psi_+^\dagger \psi_+ - \psi_-^\dagger \psi_-), \end{aligned} \quad (15)$$

where  $\psi_- = \psi_L$ ,  $\psi_+ = \psi_R$ ,  $(t, x) = (x^0, x^1)$  and  $\partial_\mu = \partial/\partial x^\mu$ . For  $h = 0$ , Eq. (15) becomes the Dirac action of a massless fermion in 1+1 dimensions, i.e.

$$\mathcal{L} = \bar{\psi} \not{\partial} \psi = \psi_-^\dagger (\partial_0 + \partial_1) \psi_- + \psi_+^\dagger (\partial_0 - \partial_1) \psi_+, \quad (16)$$

where  $\not{\partial} = \gamma^\mu \partial_\mu$ ,  $\psi^t = (\psi_-, \psi_+)$ ,  $\bar{\psi} = \psi^\dagger \gamma^0$  and  $\gamma^0 = \sigma^x$ ,  $\gamma^1 = -i\sigma^y$ . The flat space-time metric, denoted by  $\eta^{ab}$  ( $a, b = 0, 1$ ), has the signature  $(-, +)$ . Let us express Eq. (15) as the Dirac action in curved space-time. We need the space-time metric  $g_{\mu\nu}$ , the zweibein  $e_\mu^a$ , its inverse  $E_a^\mu$ , the spin connection  $\omega_\mu^{ab}$  and the Christoffel symbols  $\Gamma_{\lambda\mu}^\nu$  that are related as

$$\begin{aligned} g_{\mu\nu} &= \eta_{ab} e_\mu^a e_\nu^b, \quad E_a^\mu = g^{\mu\nu} \eta_{ab} e_\nu^b, \\ \omega_\mu^{ab} &= e_\nu^a \partial_\mu E^{b\nu} + e_\nu^b \partial_\mu E^{a\nu} - \Gamma_{\lambda\mu}^\nu E^{ab} e_\nu^\lambda. \end{aligned} \quad (17)$$

The covariant derivative on the two component spinor  $\psi$  is given by

$$D_\mu \psi = \left( \partial_\mu - \frac{1}{4} \omega_\mu^{ab} \gamma_{ab} \right) \psi, \quad (18)$$

where  $\gamma_{ab} = \frac{1}{2}[\gamma_a, \gamma_b] = -\epsilon_{ab} \sigma^z$  ( $\epsilon_{ab}$  is the Levi-Civita tensor,  $\epsilon_{01} = -\epsilon_{10} = 1$ ). The Dirac Lagrangian of a massless fermion in curved space-time reads

$$\mathcal{L} = e \bar{\psi} \not{D} \psi, \quad (19)$$

where  $\not{D} = E_a^\mu \gamma^a D_\mu$  and  $e = \det e_\mu^a$ . Assuming that  $e_\mu^a$  has only diagonal entries, and using Eqs. (17) one finds

$$e \bar{\psi} \not{D} \psi = e \psi^\dagger \left[ E_0^0 (\partial_0 + \frac{1}{2} \omega_0^{01} \sigma^z) + E_1^1 (\sigma^z \partial_1 + \frac{1}{2} \omega_1^{01}) \right] \psi, \quad (20)$$

that compared with Eq. (15) yields

$$\begin{aligned} e E_0^0 &= 1, & e E_1^1 &= e^{-h|x|}, \\ e E_0^0 \omega_0^{01} &= -h \operatorname{sign}(x) e^{-h|x|}, & \omega_1^{01} &= 0. \end{aligned} \quad (21)$$

The solution of these equations is

$$\begin{aligned} e_0^0 &= e^{-h|x|}, & e_1^1 &= 1, \\ \omega_0^{01} &= -h \operatorname{sign}(x) e^{-h|x|}, & \omega_1^{01} &= 0, \end{aligned} \quad (22)$$

that gives rise to the space-time metric

$$g_{00} = -e^{-2h|x|}, \quad g_{11} = 1. \quad (23)$$

The non vanishing components of the Christoffel symbols and the Ricci tensor are

$$\begin{aligned} \Gamma_{01}^0 &= -h \operatorname{sign}(x), & \Gamma_{00}^1 &= -h \operatorname{sign}(x) e^{-2h|x|}, \\ R_{00} &= -2h\delta(x), & R_{11} &= 2h\delta(x) - h^2, \end{aligned} \quad (24)$$

that yield the scalar curvature

$$R(x) = g^{\mu\nu} R_{\mu\nu}(x) = 4h\delta(x) - h^2. \quad (25)$$

that is constant and negative everywhere except at the origin where it is singular.

The Euclidean version of the metric (23) is

$$ds^2 = e^{2h|x|} dt^2 + dx^2 = e^{2\sigma(x)} dz d\bar{z}, \quad (26)$$

that, using Eqs. (6) and (32), coincides with Eq. (31). An alternative way to write the metric is

$$ds^2 = \frac{d\tilde{x}^2 + dt^2}{(1 + |h\tilde{x}|)^2}, \quad (27)$$

or, in terms of the variable

$$y = \tilde{x} + \frac{\operatorname{sign} \tilde{x}}{h} \longrightarrow ds^2 = \frac{dy^2 + dt^2}{h^2 y^2}, \quad (28)$$

that is the Poincaré metric in the upper-half plane in the variable  $w = y + it$ . This result is in agreement with Eq. (25) for the value of the curvature. In our case, the domain where the metric is defined consists in the union of two strips along the  $t$  axis, i.e.

$$\begin{aligned} \mathcal{P} &= \mathcal{P}_+ \cup \mathcal{P}_-, & \mathcal{P}_\pm &= \mathbb{R} \times \mathcal{I}_\pm, \\ \mathcal{I}_\pm &= \pm (y_0, y_L), & y_0 &= \frac{1}{h}, & y_L &= \frac{e^{hL}}{h}. \end{aligned} \quad (29)$$

#### 4. Entanglement entropies

The goal of this section is to show how to obtain the entanglement entropies of the rainbow chain with the methods of Ref. [31]. This will allow us to derive Eq. (11) and to generalise it to many other different bipartitions.

In the previous section we have shown that, in Lagrangian formalism (in the worldsheet  $(x, t) \in [-L, L] \times \mathbb{R}$ , with *imaginary* time  $t$ ), the 2D euclidean action corresponding to the Hamiltonian (3) is

$$\mathcal{S} = \frac{1}{2\pi} \int dz d\bar{z} e^\sigma \left[ \psi_R^\dagger \overset{\leftrightarrow}{\partial}_{\bar{z}} \psi_R + \psi_L^\dagger \overset{\leftrightarrow}{\partial}_z \psi_L \right], \quad (30)$$

in the metric

$$ds^2 = e^{2\sigma} dz d\bar{z}. \quad (31)$$

The complex coordinate  $z$ , as well as the Weyl factor  $e^\sigma$  follow from the previous section, or can be read off directly from Eq. (3),

$$\begin{aligned} z &= \tilde{x} + i t = \text{sign}(x) \frac{e^{h|x|} - 1}{h} + i t, \\ e^\sigma &= e^{-h|x|}. \end{aligned} \quad (32)$$

The complex coordinate lives on the infinite strip,  $z \in [-\tilde{L}, \tilde{L}] + i\mathbb{R}$ . This is a particular example of the general class of models considered in Ref. [31], so one can follow the arguments used in there to calculate the entanglement entropy. We will make repeated use of the standard result that the  $n^{\text{th}}$  Rényi entropy can be expressed in terms of correlation functions of twist operators in an  $n$ -times replicated worldsheet [21]. The twist field has the well known dimension [22]

$$\Delta_n = \frac{c}{12} \left( n - \frac{1}{n} \right), \quad (33)$$

where in our case  $c = 1$ .

##### 4.1. Block $A$ at the chain edge

We first consider the case of a block  $A$  starting from the edge of the chain, i.e. we focus on the bipartition

$$A = [-L, x], \quad B = [x, L]. \quad (34)$$

The Rényi entropy in this situation is related to the expectation value of a single twist operator  $\mathcal{T}_n$  at position  $(x, 0) \in [-L, L] \times \mathbb{R}$  as

$$S_{n, \text{CFT}}(x) = \frac{1}{1-n} \ln \langle \mathcal{T}_n(x, 0) \rangle_{\text{strip (curved)}}, \quad (35)$$

where  $\langle \cdot \rangle_{\text{strip (curved)}}$  stands for the expectation value in the CFT with the metric (31). Since the twist field is a primary operator with scaling dimension (33), it transforms as  $\mathcal{T}_n \rightarrow e^{-\sigma \Delta_n} \mathcal{T}_n$  under the Weyl transformation of the metric  $e^{2\sigma} dz d\bar{z} \rightarrow dz d\bar{z}$ . Thus, the expectation value of  $\mathcal{T}_n$  in curved space is related to the one in flat space through

$$\langle \mathcal{T}_n(x, 0) \rangle_{\text{strip (curved)}} = e^{-\sigma \Delta_n} \langle \mathcal{T}_n(\tilde{x}, 0) \rangle_{\text{strip (flat)}}. \quad (36)$$

The latter expectation value is entirely fixed by conformal invariance (the boundary condition for the fermions does not require insertions of boundary condition changing operators), and is easily calculated by conformally mapping the strip  $z \in [-\tilde{L}, \tilde{L}] + i\mathbb{R}$



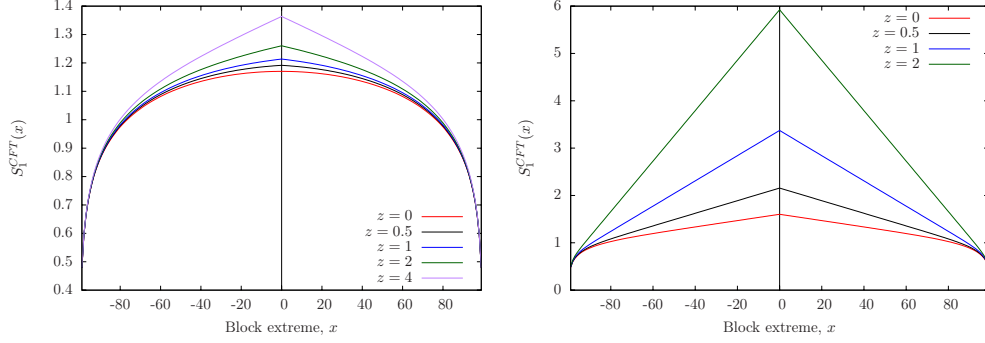


**Figure 3.** CFT prediction for the entanglement entropy  $S_1$  of the rainbow chain as given by (37) for  $L = 200$ . A part from the leading  $\ln L$  behaviour, this is a function only of  $x/L$  (horizontal axis) and  $z = hL$ . The latter is the varying parameter in the various curves which correspond to  $z = 0, 0.5, 1, 2, 4$  (left panel) and  $z = 8, 16, 32, 64$  (right panel). The two panels shows neatly the crossover from the homogeneous CFT behaviour at  $z = 0$  to the thermal like at large  $z$ .

onto the upper half-plane  $\mathbb{H}$ ,  $z \mapsto e^{i\frac{\pi}{2L}(z+\tilde{L})} \in \mathbb{H}$ . The result of this straightforward calculation is

$$S_{n,\text{CFT}}(x) = \frac{n+1}{12n} \ln Y(x), \quad (37)$$

where  $Y(x)$  is

$$Y(x) = e^\sigma \frac{8\tilde{L}}{\pi} \sin\left(\frac{\pi(\tilde{x} + \tilde{L})}{2\tilde{L}}\right) = 8e^{-h|x|} \frac{e^{hL} - 1}{\pi h} \cos\left(\frac{\pi}{2} \frac{e^{h|x|} - 1}{e^{hL} - 1}\right). \quad (38)$$

The factor 8 appearing in this expression is due to our choice of normalisation; it agrees, in the limit  $h \rightarrow 0$ , with Eq. (70) of Ref. [41] that gives the Rényi entropies of the uniform XX chain with open BC's. The term  $\frac{2\tilde{L}}{\pi} \sin(\frac{\pi(\tilde{x} + \tilde{L})}{2\tilde{L}})$  is the standard *chord distance* entering in all CFT one-point function on the infinite strip.

The half-chain entropy conjectured in Eq. (11) can be obtained from Eq. (37) setting  $n = 1$  and  $x = 0$ .

Eq. (37) shows that, apart from the leading  $\ln L$  behaviour, the Rényi entropies are just functions of  $x/L$  and  $z = hL$ . In Fig. 3 we report this universal function for the von Neumann entropy (for other Rényi only the scale changes) as function of  $x/L$  for several values of  $z$ . This figure shows the crossover from the homogeneous CFT behaviour at  $z = 0$  to the thermal like at large  $z$ . Notice in particular that for  $x$  close to the edges, one has always a logarithmic behaviour, but the region where this applies shrinks more and more as  $z$  increases.

**4.1.1. Numerical tests.** As we already mentioned, it is possible to use standard free fermion techniques [34] to calculate the Rényi entanglement entropy for an arbitrary block of the rainbow chain, as already done in [26, 27, 28]. For a block  $A$  starting from the boundary, some results of the numerical computation are reported for  $n = 1, 2, 3, 4$  in Fig. 4. We only report the results for one total length of the chain equal to  $2L = 100$  and for two values of the inhomogeneity  $h = 0.5, 0.05$ , but we have checked that other values of these parameters give equivalent results and the CFT predictions are nicely confirmed in their regime of applicability.

Just by looking at Fig. 4, it is clear that the numerical results qualitatively resemble the shape of our prediction (37) plotted in Fig. 3. However, it is also evident that on top of the smooth conformal contribution, there is an oscillating part which becomes more pronounced as the order of the Rényi entropy  $n$  increases and as  $h$  becomes smaller. Clearly, this effect is not present in the asymptotic result (37), but is a correction to scaling. These corrections to scaling are well known for homogeneous systems and have been fully characterised both for periodic [42, 43] and open systems [44, 41]. In particular in Ref. [45] it has been argued that in CFT they can be understood as arising from the insertion of relevant operators locally at the conical space-time singularity which are necessary to describe the reduced density matrix and, at half filling in a semi-infinite chain, they are of the form  $\sim f_n(-1)^x x^{-1/n}$ . It is then natural to conjecture that, also for the rainbow chain, the leading correction to the scaling is due to this relevant operator at the conical singularity and so its analytic form is obtained by employing the same conformal mapping used for calculating the leading term. Following this logic, it is straightforward to arrive to the conjecture for entanglement entropies

$$S_n(x) \simeq S_{n,\text{CFT}}(x) + S_n^{\text{osc}}(x), \quad (39)$$

where  $S_{n,\text{CFT}}(x)$  is the leading term in (37) while the oscillating part is

$$S_n^{\text{osc}}(x) = \frac{E_n}{2} + f_n \cos(\pi(x+L)) Y(x)^{-1/n}. \quad (40)$$

The constants  $E_n$  and  $f_n$  are non-universal, but, because of the previous argument based on conformal mapping, they must be the same as in the homogeneous system. Thus, from the exact solution of the homogeneous system in [41], we expect

$$f_n = \frac{2}{1-n} \frac{\Gamma(\frac{1}{2} + \frac{1}{2n})}{\Gamma(\frac{1}{2} - \frac{1}{2n})}, \quad (41)$$

while the constants  $E_n$  are complicated integrals that we do not report here (see [41, 46]) whose numerical values, for the Rényi orders we are interested in, are

$$E_{n=1,\dots,4} \approx 0.49502, 0.40405, 0.366365, 0.346061. \quad (42)$$

In Fig. 4 we compare the prediction (39) with the numerical results for  $2L = 100$ . The agreement between the two is excellent and this is particularly amazing since Eq. (39) does not contain any fitting parameter. However, at a very close look, it can be noticed a very small offset between data and prediction. This is a non-oscillating  $1/L$  correction which is known in the uniform case (see Eq. (70) in Ref. [41]), but we have been unable to conjecture a generalised form valid for all non-zero  $h$ . We repeated checks like those in Fig. 4 for several other chain length  $L$  and inhomogeneous parameter  $h$ , always finding excellent agreement.

#### 4.2. Block $A$ at an arbitrary position

We now consider the more difficult case of a single block of spins but in an arbitrary position in the chain, i.e. we consider the bipartition

$$A = [x_1, x_2], \quad B = [-L, x_1] \cup [x_2, L], \quad (43)$$

i.e.  $A$  is an interval of length  $x_2 - x_1 > 0$ . Notice that, in the central case  $x_1 = -x_2$  and in the limit  $h \rightarrow \infty$ , this block has zero entanglement given the singlet structure in Fig. 1.

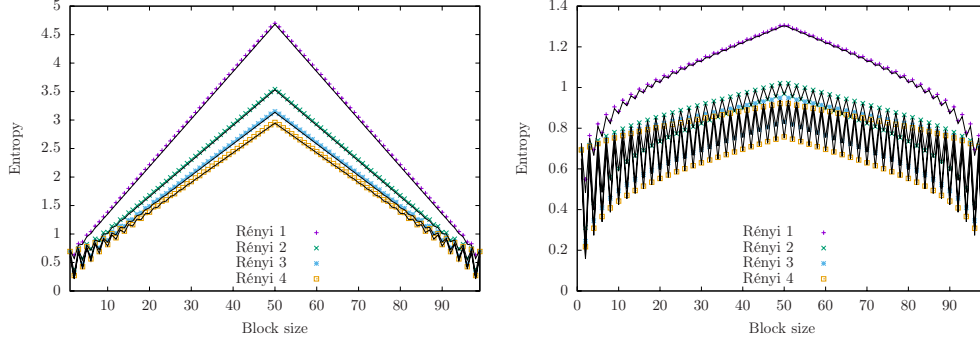


**Figure 4.** Rényi entropies  $S_n(x)$  for a system with  $2L = 100$  sites as a function of the block size  $x + L \in [1, 2L]$ . Left:  $h = 0.5$ , Right:  $h = 0.05$ . The symbols are the numerical results and the continuous lines the theoretical prediction (39).

In CFT formalism, the Rényi entropy of this interval is related to the two-point function of the twist fields  $\mathcal{T}_n, \bar{\mathcal{T}}_n$  inside the strip, which can be conformally transformed to a two-point function in the upper half-plane. Generically, the calculation of two-point functions of twist fields in the upper half plane is a very challenging problem (in fact, by method of images, it can be related to a four point function in the complex plane considered e.g. in Refs. [47, 48]). However, in the case of the massless free fermionic field-theory, this two-point function in the half plane simplifies and it becomes [49, 50, 41]

$$\langle \bar{\mathcal{T}}_n(w_1, \bar{w}_1) \mathcal{T}_n(w_2, \bar{w}_2) \rangle_{\text{uhp}} = c_n^2 \left[ \frac{|w_1 - \bar{w}_2|^2}{|w_1 - w_2|^2 |w_1 - \bar{w}_1| |w_2 - \bar{w}_2|} \right]^{\frac{1}{12}(n - \frac{1}{n})}, \quad (44)$$

where  $c_n$  is the corresponding multiplicative constant of the one point function  $\langle \mathcal{T}_n \rangle$ . This can be conformally mapped back to the strip  $(\tilde{x}, t) \in [-\tilde{L}, \tilde{L}] \times \mathbb{R}$ ; the metric on the strip is, at this point, the euclidean metric  $ds^2 = dzd\bar{z}$ . We only need the result at imaginary time  $t = 0$ , in which case the expression simplifies to

$$\langle \bar{\mathcal{T}}_n(\tilde{x}_1, 0) \mathcal{T}_n(\tilde{x}_2, 0) \rangle_{\text{strip(flat)}} = c_n^2 \left[ \frac{\frac{1}{4} \left( \frac{\pi}{2\tilde{L}} \right)^2 \cos \left( \frac{\pi(\tilde{x}_1 + \tilde{x}_2)}{4\tilde{L}} \right)^2}{\sin \left( \frac{\pi(\tilde{x}_1 - \tilde{x}_2)}{4\tilde{L}} \right)^2 \cos \left( \frac{\pi\tilde{x}_1}{2\tilde{L}} \right) \cos \left( \frac{\pi\tilde{x}_2}{2\tilde{L}} \right)} \right]^{\frac{1}{12}(n - \frac{1}{n})}.$$

Finally, we perform the Weyl transformation  $dzd\bar{z} \mapsto e^{2\sigma} dzd\bar{z}$ , which gives the two-point function we need

$$\langle \bar{\mathcal{T}}_n(\tilde{x}_1, 0) \mathcal{T}_n(\tilde{x}_2, 0) \rangle_{\text{strip(curved)}} = c_n^2 \left[ \frac{e^{-\sigma(x_1) - \sigma(x_2)} \left( \frac{\pi}{4\tilde{L}} \right)^2 \cos \left( \frac{\pi(\tilde{x}_1 + \tilde{x}_2)}{4\tilde{L}} \right)^2}{\sin \left( \frac{\pi(\tilde{x}_1 - \tilde{x}_2)}{4\tilde{L}} \right)^2 \cos \left( \frac{\pi\tilde{x}_1}{2\tilde{L}} \right) \cos \left( \frac{\pi\tilde{x}_2}{2\tilde{L}} \right)} \right]^{\frac{1}{12}(n - \frac{1}{n})}.$$

The  $n^{\text{th}}$  Rényi entropy is then

$$S_{n, \text{CFT}}(x_1, x_2) = \frac{n+1}{12n} \ln 4Y(x_1, x_2) + E_n, \quad (45)$$

with

$$Y(x_1, x_2) = \frac{e^{\sigma(x_1) + \sigma(x_2)} 16\tilde{L}^2}{\pi^2 \cos \left( \frac{\pi(\tilde{x}_1 + \tilde{x}_2)}{4\tilde{L}} \right)^2} \sin \left( \frac{\pi(\tilde{x}_1 - \tilde{x}_2)}{4\tilde{L}} \right)^2 \cos \left( \frac{\pi\tilde{x}_1}{2\tilde{L}} \right) \cos \left( \frac{\pi\tilde{x}_2}{2\tilde{L}} \right), \quad (46)$$

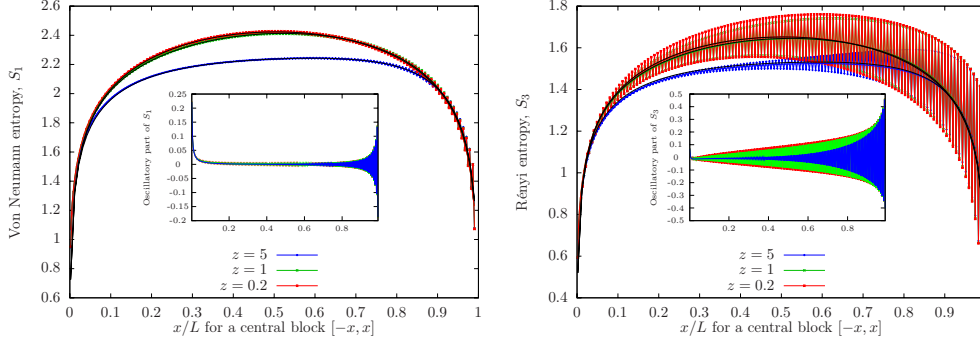


**Figure 5.** Entanglement entropies  $S_1(A)$  (left) and  $S_3(A)$  (right) for a chain with  $2L = 512$  sites and  $z = hL = 0.2, 1, 5$ . The inset of these figures shows the difference  $S_n(x) - S_{n,\text{CFT}}(x)$ , highlighting the irregular behaviour of the oscillatory part.

where, again,  $\tilde{x}_i$  and  $\tilde{L}$  are given by Eqs. (6) and (7) respectively, and  $E_n$  is given in (42). In (45) the factor 4 and the constant  $E_n$  have been fixed in order to match the exact result in the homogenous limit  $h \rightarrow 0$  obtained in [41].

**4.2.1. Numerical tests.** To be as concise as possible, we only provide numerical checks of the prediction (45) in the case of a symmetric block  $A = [x_1, x_2] = [-x, x]$  with  $x > 0$ . This bipartition is particularly interesting since in the limit  $h \rightarrow \infty$  the entanglement of this configuration vanishes because of the singlet structure (a result that we confirm numerically, but that we do not show). In Fig. 5 we report the numerically calculated entanglement entropies for this central configuration both for  $n = 1$  and  $n = 3$  and for three values of  $h$  in a regime that is intermediate between strong and weak inhomogeneity, in order to have non-trivial entropy profiles. The CFT prediction (45) is reported together with the numerical data: the agreement for the average value is really impressive considering that there are no free parameters in this comparison. However, on top of the average value well described by CFT, there are strong oscillations of the form  $(-1)^x$  times some function of  $x$ . These oscillations shares many features with those found in the case of a block starting from the edge, e.g. they are more pronounced as  $n$  increases, and they decrease with system size. In order to understand them better, or at least to guess their behaviour, we have studied the difference between the numerical  $S_n$  and the CFT prediction (45). For example, in the inset of Fig. 5, we report this difference  $S_n(x) - S_{n,\text{CFT}}(x)$  as function of the half-block size  $x$ . With system size they are compatible with a scaling  $L^{-1/n}$ , as expected from general arguments [45]. However, this scaling is multiplied by a non-trivial function of  $x$ , that, as shown in the inset of Fig. 5, grows quite strongly with  $x$ . Because of all these complications, we have not been able to obtain (or even guess) an analytic expression for them. Their shape resembles the result for the entanglement entropies in the same central configuration found in Ref. [51] for a Fermi gas trapped by a harmonic potential. In fact, also in that case it has not been possible to provide a result (or a conjecture) for their behaviour. We mention also that at a closer look at the data in the inset, it can be noticed that there is a small  $n$ - and  $h$ -dependent offset in the additive constant. This is expected to be a  $1/L$  correction similar to the one observed for the interval starting from the edge.

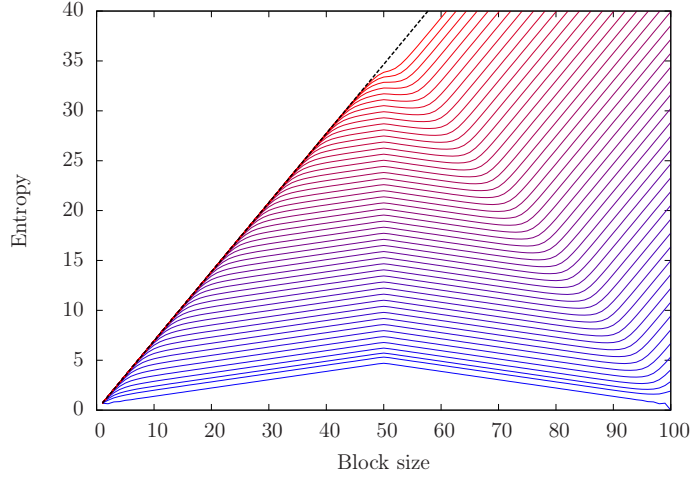


**Figure 6.** Von Neumann entanglement entropy of a rainbow state with  $2L = 100$  and  $h = 0.5$  (such that  $hL = 25 \gg 1$ ) for different physical temperatures as function of the block size  $n$ . The colours follow the increasing temperature from cold (blue) to hot (red), chosen in the following way. The lowest curve is for  $T = 0$ . As we move upwards, the  $n$ -th curve corresponds to a temperature equal to the  $n$ -th hopping starting from the left as in Eq. (47). The dashed line on the top corresponds to the maximal possible entropy for each block  $S_{\max} = n \ln 2$ .

## 5. Rainbow state at finite temperature

A final question one naturally poses when studying the rainbow chain is what happens at finite temperature. Given that for  $hL \gg 1$  the effect of the inhomogeneity is the same as a large temperature, it is particularly interesting to address the combined effect of this effective temperature (14) and a real external one. Calculating the entanglement entropy at finite temperature in our problem is very difficult. Indeed, the topology that one should study is the one of an annulus with two open boundaries in the real space coordinate and periodic conditions along the imaginary time. Calculating either one- or two-point correlation function of twist fields in this geometry is an advanced problem that lies beyond the scope of this manuscript. On the other hand, the most interesting effect we are aiming to describe (i.e. the interplay between real and effective temperature) takes place in the limit  $hL \gg 1$  where the physics considerably simplifies and we are able to fully characterise it on the sole basis of the numerics.

In Fig. 6 we report the effect of the physical temperature on a rainbow chain with  $2L = 100$  sites for a high value of  $h = 0.5$  (such that  $hL = 25 \gg 1$ ). Fig. 6 shows the von Neumann entropy of blocks starting from the left boundary, as a function of the block size. The set of temperatures, nonetheless, have been chosen with care. The lowest curve corresponds to  $T = 0$ , and exhibits the usual tent shape, with a slope approximately equal to  $h/6$  (recall Eq. (12)). Above this curve, the  $n$ -th one corresponds to a temperature equal to the  $n$ -th hopping, counting from the left end, i.e.

$$T_n = e^{-h(L-1/2-n)}, \quad n = 1, \dots, L-1. \quad (47)$$

The dotted curve corresponds to the maximal possible entropy for each block size,

that is  $n \ln 2$  (in this section we only consider the von Neumann entropy and so we denote the site with  $n$  without risking to make confusion with the Rényi index).

The results in Fig. 6 show that for fixed finite temperature there are three linear behaviours (except at the turning points where some crossover takes place quite rapidly) with slopes that can be explained in the following way. Let us assume that we set the physical temperature equal to the hopping at a certain point  $x_0 > 0$  (and its reflection,  $-x_0$ ):  $T = J(x_0)$ . The blocks lying on the left edge, i.e.  $(-L, x)$  with  $x < -x_0$ , involve hopping amplitudes much lower than the temperature, that is  $J(x) \ll T$ , and hence the entropy will be maximal and given approximately by  $(L - |x|) \ln 2$ . When the right point of the block  $(-L, x)$  moves past  $-x_0$ , now the local hopping is much larger than the temperature,  $J(x) \gg T$ , and the behaviour of the entropy is as in the zero-temperature case. Finally, when  $x > x_0$ , one gets  $J(x) \ll T$ , and the entropy growth is again the maximal one. Summarising, we have

$$S(x) \sim \begin{cases} (L - |x|) \ln 2, & x \in (-L, -x_0), \\ (L - x_0) \ln 2 + (x_0 - |x|)h/6, & x \in (-x_0, x_0), \\ (L - 2x_0 + x) \ln 2, & x \in (x_0, L). \end{cases} \quad (48)$$

In other terms: if the right extreme of the block is in the interval  $[-x_0, x_0]$ , the behaviour will be similar to the zero temperature case, and if it is outside that region, it will correspond to infinite temperature. Thus, the various curves can be just characterised by the value they have at  $x = 0$ , i.e. by the half-chain entropy. According to the previous argument, we have for a rainbow system with a given  $h$  (such that  $hL \gg 1$ ) and physical temperature  $T$ , the half-chain entropy (recall  $T = J(x_0) = e^{-hx_0}$ )

$$S(x=0) \simeq \left( \frac{\ln 2}{h} - \frac{1}{6} \right) \ln T + L \ln 2. \quad (49)$$

The correctness of this prediction is checked in Fig. 7. The range of validity of the approximation is for  $T$  within the range of values for the hopping, i.e. if it exists  $x_0$  such that  $T = J(x_0)$ . Notice that, for  $h = 0.2$ , this range is more reduced.

## 6. Conclusions

In this paper we applied methods of 2d quantum field theory in curved space-time to the study of the *rainbow chain*, which has a ground state that for  $hL \gg 1$  possesses a volume law, analogous to a thermal state with large temperature  $T_R = h/(2\pi)$ .

We first showed that the rainbow system is describable by a massless Dirac fermion on a Riemannian manifold with constant negative curvature everywhere except at the centre, equivalent to a Poincaré metric with a strip removed. This identification allowed us to apply the recent results of Ref. [31] to the rainbow state. In this way, we provided accurate predictions for the smooth part of the entanglement entropies of blocks of different types which perfectly describe the numerical data. We also conjectured a precise form for the oscillatory part of the entropies in the case of edge blocks.

The dynamics of the rainbow state at finite temperature is also very peculiar. For  $T$  in the range of energies spanned by the values of the hopping amplitude, we showed that the system splits into three regions: the central one behaves as if it were at  $T = 0$ , while the two extremes as if they were at  $T = \infty$ .

There are still many more results that can be derived by using the curved CFT approach and that can help understand the structure of the rainbow model. For

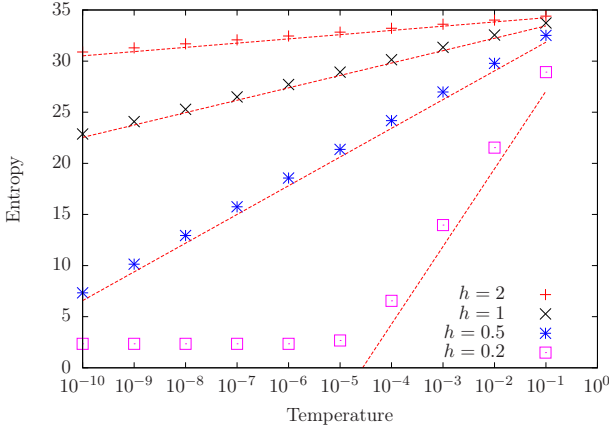


**Figure 7.** Entanglement entropy of the half chain as a function of the temperature for rainbow chains with  $2L = 100$  and different values of  $h$ . The dashed red line is the theoretical approximation (49). Notice that the approximation is correct as long as the temperature lies within the range of hoppings. For  $h = 0.2$  it fails for  $T \approx 10^{-5}$ , because these temperatures are below the minimum hopping.

examples, it should be easy to generalise the results presented here for the ground state to excited states, both low lying ones and those in the middle of the spectrum. For the former, one can use the universal CFT approach [52, 53], while for the latter one can exploit the results in [54]. Another possible generalisation is to consider other entanglement measures that have a CFT representation such as bipartite fidelity [55], entanglement negativity [56], and relative entropies [57].

Moving away from the rainbow, the dynamics of conformal fields on curved backgrounds provides a rich source of physical phenomena to explore, whose interest is growing due to the recent proposals of experimental realisations in, e.g., ultracold atoms on optical lattices [29, 30]. The subtle interplay between entanglement and geometry helps explain the thermal effects in quantum field theory on curved backgrounds, e.g. the Unruh effect or the local temperature effects in inhomogeneous fermionic systems [58].

## Acknowledgements

We would like to thank A. Abanov, L. Alvarez-Gaumé, V. Korepin, E. López, J. Mas, G. Mussardo, E. Tonni, J. Pachos, A. Ramallo and T. Takayanagi for useful comments. This work was funded by grants FIS-2012-33642, FIS-2012-38866-C05-1, and FIS2015-69167-C2-1-P from the Spanish government, QUITEMAD+ S2013/ICE-2801 from the Madrid regional government and SEV-2012-0249 of the Centro de Excelencia Severo Ochoa Programme. J.D. and G.S. thank Nordita, Stockholm, for hospitality during the Workshop “From quantum field theories to numerical methods”, where part this work was done. J.D. acknowledges financial support from CNRS “Défi Inphyniti” and from the Conseil Régional and Université de Lorraine. G. S. thanks SISSA for hospitality during the starting stage of this project. P.C. acknowledges funding from the ERC under Starting Grant 279391 EDEQS.



## References

- [1] L. Amico, R. Fazio, A. Osterloh, and V. Vedral, *Rev. Mod. Phys.* **80**, 517 (2008).
- [2] J. Eisert, M. Cramer, M. B. Plenio, *Rev. Mod. Phys.* **82**, 277 (2010).
- [3] P. Calabrese, J. Cardy, and B. Doyon Eds, *J. Phys. A* **42** 500301 (2009).
- [4] N. Laflorencie, *Phys. Rep.* **643**, 1 (2016).
- [5] R. Islam, R. Ma, P. M. Preiss, M. E. Tai, A. Lukin, M. Rispoli, and M. Greiner, *Nature* **528**, 77 (2015).
- [6] A. M. Kaufman, M. E. Tai, A. Lukin, M. Rispoli, R. Schittko, P. M. Preiss, and M. Greiner, *Science* **353**, 794 (2016).
- [7] J. Cardy, *Phys. Rev. Lett.* **106**, 150404 (2011).
- [8] D. A. Abanin and E. Demler, *Phys. Rev. Lett.* **109**, 020504 (2012).
- [9] A. J. Daley, H. Pichler, J. Schachenmayer, and P. Zoller, *Phys. Rev. Lett.* **109**, 020505 (2012).
- [10] H. Pichler, G. Zhu, A. Seif, P. Zoller, and M. Hafezi, *Phys. Rev. X* **6**, 041033 (2016).
- [11] V. Alba, [arXiv:1609.02157](#).
- [12] J. Unmuth-Yockey, Jin Zhang, P.M. Preiss, Li-Ping Yang, S.-W. Tsai, and Y. Meurice, [arXiv:1611.05016](#).
- [13] G. Refael and J. E. Moore, *Phys. Rev. Lett.* **93**, 260602 (2004).
- [14] G. Refael and J. E. Moore, *J. Phys. A* **42**, 504010 (2009).
- [15] N. Laflorencie, *Phys. Rev. B* **72**, 140408 (2005).
- [16] M. Fagotti, P. Calabrese, and J. E. Moore, *Phys. Rev. B* **83**, 045110 (2011).
- [17] G. Ramírez, J. Rodríguez-Laguna and G. Sierra, *J. Stat. Mech.* P07003 (2014).
- [18] P. Ruggiero, V. Alba, and P. Calabrese, *Phys. Rev. B* **94**, 035152 (2016).
- [19] C. Holzhey, F. Larsen and F. Wilczek, *Nucl. Phys. B* **424**, 443 (1994).
- [20] G. Vidal, J. I. Latorre, E. Rico and A. Kitaev, *Phys. Rev. Lett.* **90** 227902 (2003).
- [21] P. Calabrese and J. Cardy, *J. Stat. Mech.* P06002 (2004).
- [22] P. Calabrese and J. Cardy, *J. Phys. A* **42**, 504005 (2009).
- [23] K. Okunishi and T. Nishino, *Phys. Rev. B* **82**, 144409 (2010).
- [24] H. Ueda and T. Nishino, *J. Phys. Soc. Japan* **78**, 014001 (2009).
- [25] H. Ueda, H. Nakano, K. Kusakabe, and T. Nishino, *Prog. Theor. Phys.* **124**, 389 (2010).
- [26] G. Vitagliano, A. Riera, and J. I. Latorre, *New J. Phys.* **12**, 113049 (2010).
- [27] G. Ramírez, J. Rodríguez-Laguna and G. Sierra, *J. Stat. Mech.* P10004 (2014).
- [28] G. Ramírez, J. Rodríguez-Laguna and G. Sierra, *J. Stat. Mech.* P06002 (2015).
- [29] O. Boada, A. Celi, J. I. Latorre, and M. Lewenstein, *New J. Phys.* **13**, 035002 (2011).
- [30] J. Rodríguez-Laguna, L. Tarruell, M. Lewenstein, and A. Celi, [arXiv:1606.09505](#).
- [31] J. Dubail, J.-M. Stéphan, J. Viti, P. Calabrese, [arXiv:1606.04401](#).
- [32] P. Calabrese and A. Lefevre, *Phys. Rev. A* **78**, 032329 (2008).
- [33] C. Dasgupta and S.-K. Ma, *Phys. Rev. B* **22**, 1305 (1980).
- [34] I. Peschel, *J. Phys. A* **36**, L205 (2003);  
I. Peschel and V. Eisler, *J. Phys. A* **42**, 504003 (2009).
- [35] L. Bombelli, R. K. Koul, J. Lee, R. D. Sorkin, *Phys. Rev. D* **34**, 373 (1986);  
M. Srednicki, *Phys. Rev. Lett.* **71**, 666 (1993).
- [36] M. M. Wolf, F. Verstraete, M. B. Hastings, J. I. Cirac, *Phys. Rev. Lett.* **100**, 070502.
- [37] M. B. Hastings, *J. Stat. Mech.* P08024 (2007).
- [38] M. M. Wolf, *Phys. Rev. Lett.* **96**, 010404 (2006).
- [39] D. Gioev and I. Klich, *Phys. Rev. Lett.* **96**, 100503 (2006).
- [40] P. Calabrese, M. Mintchev, and E. Vicari, *Europhys. Lett.* **97**, 20009 (2012).
- [41] M. Fagotti and P. Calabrese, *J. Stat. Mech.* P01017 (2011).
- [42] P. Calabrese, M. Campostrini, F. Essler and B. Nienhuis, *Phys. Rev. Lett.* **104**, 095701 (2010).
- [43] P. Calabrese and F. H. L. Essler, *J. Stat. Mech.* P08029 (2010).
- [44] N. Laflorencie, E. S. Sorensen, M.-S. Chang, and I. Affleck, *Phys. Rev. Lett.* **96**, 100603 (2006).
- [45] J. Cardy and P. Calabrese, *J. Stat. Mech.* P04023 (2010).
- [46] B.-Q. Jin and V.E. Korepin, *J. Stat. Phys.* **116**, 79 (2004).
- [47] S. Furukawa, V. Pasquier, and J. Shiraishi, *Phys. Rev. Lett.* **102**, 170602 (2009).
- [48] P. Calabrese, J. Cardy, and E. Tonni, *J. Stat. Mech.* P11001 (2009);  
P. Calabrese, J. Cardy, and E. Tonni, *J. Stat. Mech.* P01021 (2011).
- [49] H. Casini, C. D. Fosco, and M. Huerta, *J. Stat. Mech.* P07007 (2005).
- [50] P. Calabrese, M. Mintchev, and E. Vicari, *Phys. Rev. Lett.* **107**, 020601 (2011);  
P. Calabrese, M. Mintchev, and E. Vicari, *J. Stat. Mech.* P09028 (2011).
- [51] P. Calabrese, P. Le Doussal, and S. N. Majumdar, *Phys. Rev. A* **91**, 012303 (2015).
- [52] F. C. Alcaraz, M. Ibanez Berganza, and G. Sierra, *Phys. Rev. Lett.* **106**, 201601(2011);



- M. Ibanez Berganza, F. C. Alcaraz, G. Sierra, [J. Stat. Mech. P01016 \(2012\)](#).
- [53] L. Taddia, J. C. Xavier, F. C. Alcaraz, and G. Sierra [Phys. Rev. B 88, 075112 \(2013\)](#);  
L. Taddia, F. Ortolani, and T. Palmai, [J. Stat. Mech. \(2016\) 093104](#).
- [54] V. Alba, M. Fagotti, and P. Calabrese, [J. Stat. Mech. P10020 \(2009\)](#).
- [55] J. Dubail and J.-M. Stephan, [J. Stat. Mech. \(2011\) L03002](#).
- [56] P. Calabrese, J. Cardy, and E. Tonni, [Phys. Rev. Lett. 109, 130502 \(2012\)](#);  
P. Calabrese, J. Cardy, and E. Tonni, [J. Stat. Mech. P02008 \(2013\)](#).
- [57] N. Lashkari, [Phys. Rev. Lett. 113, 051602 \(2014\)](#);  
N. Lashkari, [Phys. Rev. Lett. 117, 041601 \(2016\)](#).
- [58] S. Robles and J. Rodriguez-Laguna, [ArXiv:1609.01154](#).